Highly Excited States in C^{11}. Elastic Scattering of Protons by B^{10}†

J. C. Overley* and Ward Whaling

California Institute of Technology, Pasadena, California

(Received May 21, 1962)

Excitation functions for the elastic scattering of protons by B^{10} have been measured at center-of-mass scattering angles near 90°, 125°, and 160° for proton energies between $E_p=0.15$ MeV and $E_p=3.0$ MeV. Scattering angular distributions were measured at 43 selected energies in this range. An excitation function for the reaction $B^{10}(p,\alpha_0)Be^7$ was also measured between $E_p=1.5$ MeV and $E_p=2.6$ MeV at a laboratory angle of 90°. The atomic stopping cross section of boron for protons has been determined between $E_p=0.1$ MeV and $E_p=3.0$ MeV.

The elastic scattering excitation functions exhibit conspicuous anomalies at $E_p=1.50$ MeV and $E_p=2.180$ MeV. The α_0 transition to the ground state of Be^7 is also resonant at $E_p=2.180$ MeV. The behavior of the cross sections in these regions has been analyzed in terms of compound states of C^{11}. Satisfactory agreement is achieved with level assignments of $J^\pi=7/2^+$ with $E_R=1.50$ MeV, $\Gamma_p=90$ keV, $\Gamma_T=250$ keV; and $J^\pi=9/2^+$ with $E_R=2.180$ MeV, $\Gamma_p=100$ keV, $\Gamma_{\alpha 0}=100$ kev, and $\Gamma_T=200$ keV. Although complete analysis of the scattering is hindered by the influence of unknown background processes, the negative parity assignment for the previously reported state at $E_p=1.17$ MeV, derived from other reaction experiments, appears inconsistent with the scattering.

I. INTRODUCTION

THE observation of neutron groups from the stripping reaction $B^{10}(d,n)C^{11}$ has indicated the presence of states in C^{11} at excitation energies $E_x=8.97\pm0.02$, 9.69 ± 0.03, 10.09 ± 0.02, 10.89 ± 0.02 MeV, and perhaps also at $E_x=9.13\pm0.02$, 9.28 ± 0.02, 10.69 ± 0.02, and 11.26 ± 0.02 MeV.[1] This region of excitation has also been investigated through the reactions $B^{10}(p,\gamma)B^{11}$, $B^{10}(p,\alpha_0)Be^7$, $B^{10}(p,\alpha_1)Be^{7*}$, but there remains uncertainty concerning the spins and parities, and indeed even the existence, of most of these states. Only the states at $E_x=9.69$ and 10.09 MeV have been observed in the $B^{10}+p$ reactions, and there are conflicting spin and parity assignments for the 9.69-MeV state. The nature of these ambiguities can be best illustrated by the following experimental results.

For proton energies of less than 3 MeV, the yield of γ rays to the ground state of C^{11} ($J^\pi=3/2^-$) exhibits a resonance with a total width of approximately 500 keV near a proton energy $E_p=1.14$ MeV, indicating a state of C^{11} at $E_x=9.74$ MeV.[2,3] Above $E_p=1.8$ MeV, the cross section for this process increases rapidly, but shows no evidence of structure. In the region of the resonance, γ-cascade transitions have been observed through states with excitation energies $E_x=6.50$ MeV and 4.26 MeV, which are thought to have assignments $J^\pi=7/2^-$ and $5/2^-$, respectively.[4] The constant relative intensities of these three γ transitions for proton energies between $E_p=0.75$ MeV and $E_p=1.30$ MeV,

and the lack of forward-backward asymmetry in the angular distributions at $E_p=1.16$ MeV, suggest that the transitions proceed from a single parent state in C^{11}. The absolute intensities indicate that all three transitions are dipole in character, limiting the spin of the parent state to $J=5/2$. A strong $\cos^2\theta$ dependence in the angular distributions of the gamma rays, particularly for the $E_x=9.74$ MeV to 6.50 MeV transition, indicates that the state is formed by p-wave protons and is therefore of odd parity. The assignment of the 9.74-MeV state is fixed at $J^\pi=5/2^-$.

The α_0-particle decay to the ground state of Be^7 ($J^\pi=3/2^-$), which has been investigated for proton energies from $E_p=0.06$ MeV to $E_p=1.63$ MeV, exhibits resonances near $E_p=1.17$ and 1.5 MeV, corresponding to states of C^{11} at $E_x=9.76$ and 10.09 MeV. The α_0-particle angular distributions are nearly isotropic below $E_p=1.2$ MeV, but at higher energies show a dependence on $P_1(\cos\theta)$ and $P_3(\cos\theta)$ which reaches a maximum near $E_p=1.36$ MeV.[5] The presence of these odd Legendre polynomials has been interpreted as evidence that the states at $E_x=9.7$ and 10.09 MeV have opposite parities. The α_1 decay to the first excited state of Be^7 ($J^\pi=1/2^-$), which has been studied up to $E_p=3.0$ MeV through the reactions[5,3] $B^{10}(p,\alpha_1)Be^{7*}$ and $B^{10}(p,\alpha_1\gamma)Be^7$, is resonant only at $E_p=1.5$ MeV. The preferred assignment for the 10.09-MeV state is $J^\pi=7/2^+$ formed by s- and d-wave protons and decaying by $l=3$ alpha particles. This assignment is consistent with roughly equal strengths of the two α decays and the failure to observe the γ transition to the ground state of C^{11}.

If the $J^\pi=7/2^+$ assignment for the 10.09-MeV state is correct, and if the α_0-particle angular distributions have been properly interpreted, the parity of the 9.76-MeV state must be odd. An assignment $J^\pi=3/2^-$, with the state formed by p-wave protons and decaying

[1] F. Ajzenberg-Selove and T. Lauritsen, Nuclear Phys. 11, 105–111 (1959).
[2] G. B. Chadwick, T. K. Alexander, and J. B. Warren, Can. J. Phys. 34, 381 (1956).
[3] S. E. Hunt, R. A. Pope, and W. W. Evans, Phys. Rev. 106, 1012 (1957).
[4] A. N. James, Nuclear Phys. 24, 675 (1961).
[5] J. W. Cronin, Phys. Rev. 101, 298 (1956).

by s-wave α_0 particles, is the only one compatible with both the α_0-particle isotropy at low energies and the γ-ray anisotropy. Unfortunately, however, this assignment is inconsistent not only with that derived from the γ decay of the state, but also with the α_0-particle angular distributions near $E_p=1.36$ MeV, since it is not possible to obtain a $P_1(\cos\theta)$ term in an angular distribution from interference between $J^\pi=7/2^+$ and $J^\pi=3/2^-$ states with the properties listed above. Furthermore, a total width of 300 keV for the state obtained from the α_0-excitation curve, is incompatible with the width obtained from the γ-ray decay.

In an attempt to resolve some of the questions about these two states, and to verify the existence of the others, the elastic scattering of protons by B^{10} has been studied for proton energies from $E_p=0.150$ MeV to $E_p=3.0$ MeV. Although this experiment had been performed previously over limited energies at one scattering angle,[6] no detailed analysis of the scattering in terms of compound states in C^{11} was made. One source of uncertainty in most of the previous experiments on the proton induced reactions has been eliminated from this work through measurement of the atomic stopping cross section of boron for protons. To facilitate analysis of the scattering at high proton energies, the excitation function for the ground-state alpha decay has been extended from $E_p=1.5$ to 2.6 MeV.

II. EQUIPMENT

Two electrostatic generators with their associated analyzing equipment were used in this experiment. For proton energies below 650 keV, the Kellogg Radiation Laboratory 700-kV generator was used; for higher energies, the 3.0-MV accelerator was employed. The energy of the incident protons was determined to $\pm 0.1\%$ by electrostatic analyzers calibrated against
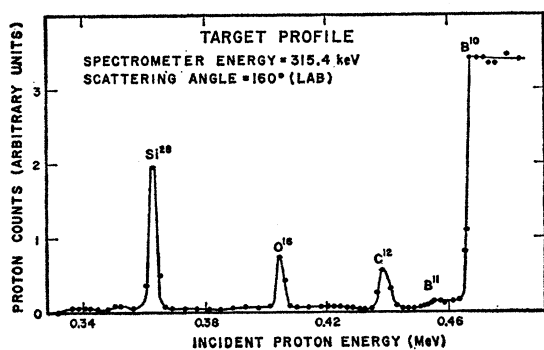

FIG. 1. The yield of protons of fixed energy scattered from a B^{10}-enriched target is shown as a function of incident proton energy. The peaks attributed to scattering from Si^{28}, O^{16}, and C^{12} are due to contaminations from the cracking of pump oil vapors on the target surface.

the $F^{19}(p,\alpha\gamma)O^{16}$ resonance at $E_p=340.5$ keV, the $Al^{27}(p,\gamma)Si^{28}$ resonance at $E_p=992$ keV, and the $Li^7(p,n)Be^7$ threshold at $E_p=1.881$ MeV. Scattered protons were analyzed in double-focusing magnetic spectrometers with resolutions of the order of 0.2% in energy and solid angles of approximately 0.006 sr subtended at the target. The spectrometers were calibrated against analyzed protons elastically scattered from freshly evaporated copper targets, and also from carbon surface contaminations which were deposited on the boron targets through decomposition of organic vapors in the vacuum system. The amount of charge incident on the target was measured to within $\pm 0.3\%$ by a conventional current integrator.

Elastically scattered protons were detected by a thin (0.015 in.) cesium iodide crystal mounted directly on the face of a photomultiplier tube behind the exit slits of the spectrometer. To detect alpha particles from the $B^{10}(p,\alpha)Be^7$ reaction in the presence of scattered protons which have the same energy as the alpha particles at some angles of observation and bombarding energy, the scintillation detector was replaced by a solid-state detector. The two particle groups were resolved by preferentially degrading the energy of the α particles with a 10 000-Å nickel foil placed at the exit slits of the spectrometer.

B^{10} targets were made by thermally decomposing diborane (B_2H_6) onto polished tungsten blanks by inductively heating the blanks to approximately 600°C in an atmosphere of B_2H_6. The B_2H_6 was made from a complex $(CaF_2 \cdot BF_3)$ in which the boron had been enriched to 95.96% B^{10}. This isotopic assay was made by the supplier of the complex,[7] who estimated an error of less than 1% from known sources of systematic error. The composition was checked by analyzing the energy spectrum of protons elastically scattered from the targets. Such a "profile" of a thick target is shown in Fig. 1, where the yield of scattered protons of constant energy is plotted as a function of incident proton energy. These profiles indicated negligible amounts of heavy-element contamination and gave a relative B^{10}, B^{11} concentration consistent with the supplier's assay. Liquid nitrogen traps in the target chamber minimized the buildup of target surface contaminations from the cracking of organic pump oil vapors. At low proton energies, where the effects of surface contamination can be particularly serious, the targets were heated electrically.

III. ELASTIC SCATTERING

Excitation functions for the elastic scattering of protons by B^{10} were measured at center-of-mass angles θ_c near 90°, 125°, and 160° for proton energies from $E_p=0.150$ to 3.0 MeV. In this energy range, 43 angular

[6] A. B. Brown, C. W. Snyder, W. A. Fowler, and C. C. Lauritsen, Phys. Rev. 82, 159 (1951).

[7] Oak Ridge National Laboratory, Stable Isotopes Division, Oak Ridge, Tennessee.
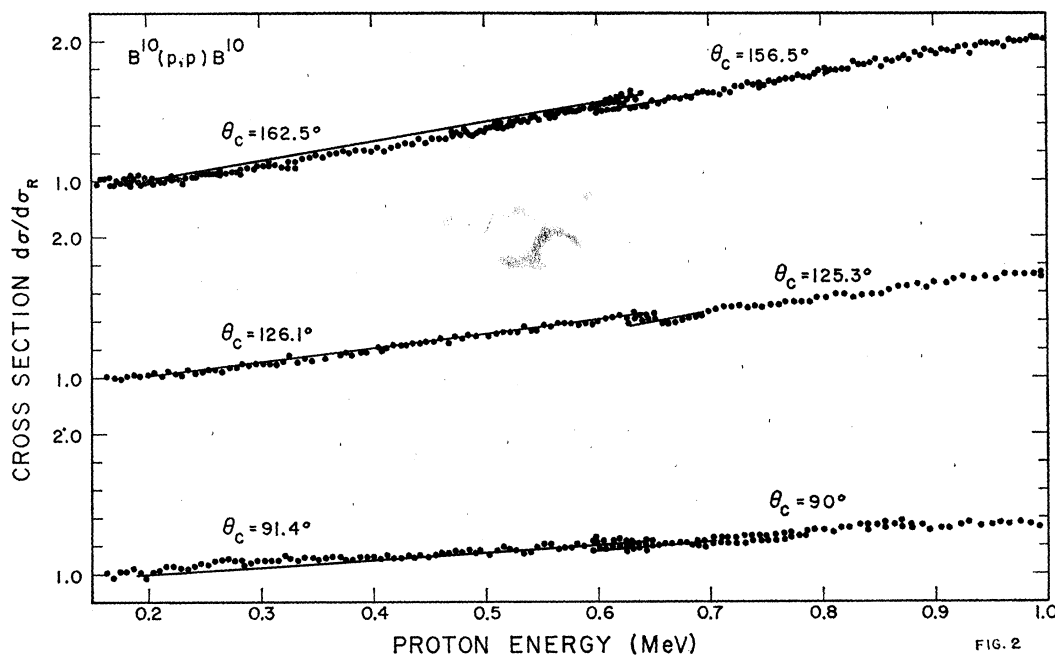
FIG. 2. Excitation functions for $B^{10}(p,p)B^{10}$ from $E_p=0.150$ to $E_p=1.0$ MeV, including the region from $E_p=600$ keV to $E_p=650$ keV where data taken with the two accelerators overlaps. The curves represent the best theoretical fits obtained for pure s-wave potential scattering.

distributions were also measured, with experimental points at 10° intervals from $\theta_c=60°$ to $\theta_c=150°$.

The yield of protons scattered by B^{10} was determined by counting particles from the top of the B^{10} step in the thick-target profile. The incident energy and spectrometer energy were set at values corresponding to points approximately 2% in energy behind the midpoint of the rise. At these settings, protons scattered by the B^{10} in a thin lamina just inside the front surface of the target were detected. The energy of these protons immediately before scattering was computed from the incident energy, the spectrometer energy, and the atomic stopping cross section of boron for protons. Background counts, due primarily to protons scattered from the B^{11} contamination, were determined by measuring the yield just in front of the B^{10} step. This background was found to be a slowly varying function of energy which was subtracted from the yield at the top of the step to determine the yield of protons scattered by B^{10} alone.

The B^{10} scattering yield, Y, was converted to a laboratory cross section by applying[8]

$$\frac{d\sigma(E_1)}{d\Omega}=K\frac{Y}{E_{20}}\left[\epsilon(E_{10})\frac{\partial E_2}{\partial E_1}+\epsilon(E_{20})\frac{\cos\theta_1}{\cos\theta_2}\right], \quad (1)$$

where θ_1 and θ_2 are the angles between the target normal and the incident and scattered proton beams, and

$\epsilon(E_{10})$ and $\epsilon(E_{20})$ are the stopping cross sections per B^{10} atom at the incident energy E_{10} and the spectrometer energy E_{20}. The derivative $\partial E_2/\partial E_1$, where E_1 is the proton energy immediately before scattering and E_2 is the energy immediately after scattering, is determined by the kinematics. The quantity K, which depends on the spectrometer resolution and solid angle, the number of protons incident on the target, and the detection efficiency, was determined from the proton scattering yield from copper by assuming that the copper scattering cross section is described by classical Coulomb scattering with (at low energies) electron screening corrections.[9] At low energies, K also involves the ratio of neutral to charged hydrogen ions emergent from the target. It was assumed that this ratio was determined by the target surface contaminations and that values of K determined from copper were therefore also applicable to the calculation of the boron scattering cross section. Measurements of K at intervals of 10% of the incident proton energy were interspersed with measurements of the B^{10} scattering yield to minimize the effects of electronic drifts and possible changes in detection efficiency with energy.

Excitation curves for the ratio, $d\sigma/d\sigma_R$, of the experimental elastic scattering cross section to the calculated Coulomb cross section, are shown in Figs. 2 and 3. These curves are dominated by strong anomalies at proton energies near $E_p=1.5$ and 2.2 MeV. Above

[8] C. W. Snyder, S. Rubin, W. A. Fowler, and C. C. Lauritsen, Rev. Sci. Instr. 21, 852 (1950).

[9] W. A. Wenzel and W. Whaling, Phys. Rev. 87, 499 (1953).

$B^{10}(p,p)B^{10}$ EXCITATION FUNCTIONS

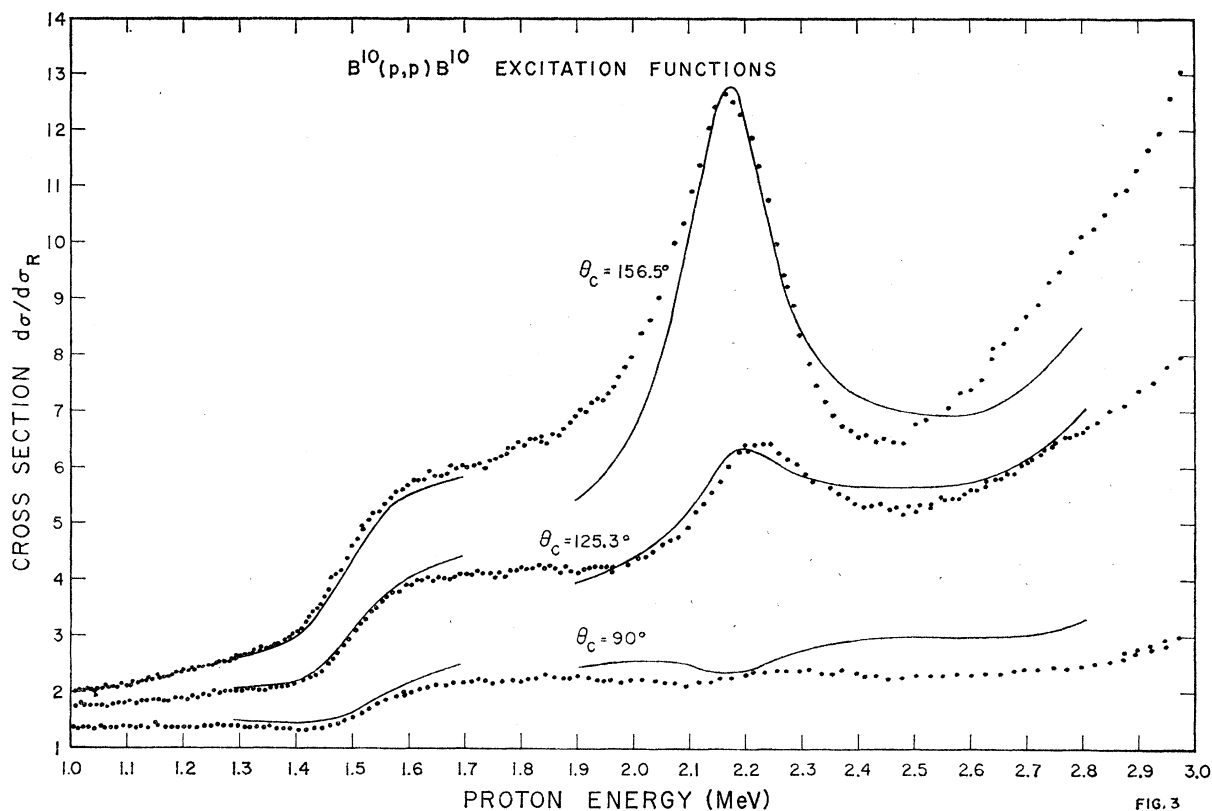CROSS SECTION $d\sigma/d\sigma_R$

PROTON ENERGY (MeV)

FIG. 3

FIG. 3. Excitation functions for $B^{10}(p,p)B^{10}$ from $E_p=1.0$ MeV to $E_p=3.0$ MeV. The curves between $E_p=1.3$ MeV and $E_p=1.7$ MeV represent theoretical values from a $J^\pi=7/2^+$ state resonant at $E_p=1.50$ MeV, superimposed on a broad $J^\pi=5/2^+$ state resonant at $E_p=1.17$ MeV. The curves between $E_p=1.9$ MeV and $E_p=2.8$ MeV represent theoretical values for a $J^\pi=9/2^+$ state at $E_p=2.18$ MeV interfering with a $J^\pi=7/2^+$ state resonant at $E_p=2.8$ MeV.

$E_p=2.6$ MeV, the cross section rises at all angles which suggests a resonant state (or states) at high proton energies. Examples of the experimental angular distributions are shown in Fig. 4.

The values of the cross section obtained with pure boron targets were checked by measuring the relative scattering yields from oxygen and B^{10} in a B_2O_3 target, enriched[7] in boron content to 94% B^{10}. The target was prepared in the target chamber by evaporating fused B_2O_3 onto a polished beryllium blank. The correction to the oxygen scattering yield due to surface contaminations of oxygen were estimated from the amount of contamination observed on a clean beryllium target. Profiles of these two targets are shown in Fig. 5. The B^{10} scattering cross section was determined from the previously measured O^{16} scattering cross section[10] by application of Eq. (1), where the O^{16} yield was used to determine K. The advantage of this method is that values of the cross section so obtained do not depend strongly on the condition of the target surface or on the absolute values of the B_2O_3 stopping cross section for protons. This molecular stopping cross section was

computed from values of the atomic stopping cross sections of boron and oxygen.[11] The major uncertainty in this measurement is the relative concentrations of O^{16} and B^{10}.

At $E_p=1.250$ MeV and $\theta_c=125.3°$, the elastic-scattering cross section obtained with the B_2O_3 target (relative to the Coulomb cross section) is $d\sigma/d\sigma_R=2.07$ ±0.08, whereas that obtained from the pure boron target is $d\sigma/d\sigma_R=1.86\pm0.13$. Since these values overlap within the estimated probable errors, the agreement is considered satisfactory.

At sufficiently low energies, the scattering cross section may be expected to approach the Coulomb value. Below 200 keV, the cross section ratio measured with the pure boron target remains constant at all angles at $d\sigma/d\sigma_R=0.94$. If these cross sections are all increased by 6% to normalize them to unity below 200 keV, the cross section ratio becomes $d\sigma/d\sigma_R=1.97$ at $E_p=1.250$ MeV and $\theta_c=125.3°$, which is very nearly the mean of the two measured values above. It is these normalized cross sections that are shown in Figs. 2 and 3. The 6% normalization factor lies within the estimated probable error of the measurements.

[10] F. J. Eppling, Massachusetts Institute of Technology Laboratory for Nuclear Science, Annual Progress Report No. 88, June 1, 1954–May 31, 1955 (unpublished).

[11] W. Whaling, *Handbuch der Physik*, edited by S. Flügge (Springer-Verlag, Berlin, 1958), Vol. 34, p. 193.

The accuracy of the energy dependence of the cross sections is estimated at $\pm 2\%$, the errors being due primarily to counting statistics and background subtractions, and the absolute probable error is estimated at $\pm 7\%$, due primarily to the errors of $\pm 4\%$ in the absolute values of the stopping cross sections of boron and copper. Other systematic errors are estimated at less than 1%, a contention supported by the results obtained from the different accelerators in the region between $E_p = 600$ keV and $E_p = 650$ keV (Fig. 2), which agree to within 1% when the small difference in scattering angle is taken into account.
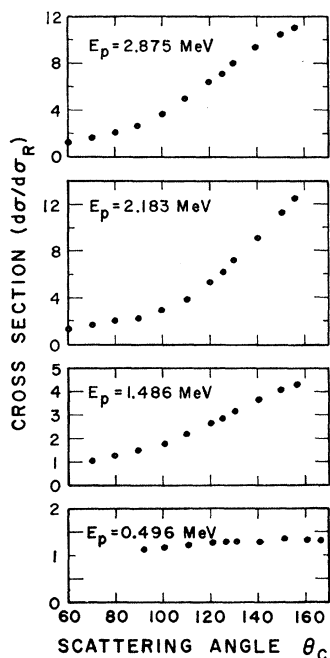

FIG. 4. Typical examples of experimental angular distributions for the elastic scattering of protons by B[10].

IV. THE STOPPING CROSS SECTION

The conversion of thick target yields into cross sections requires knowledge of the appropriate stopping cross sections. The atomic stopping cross section of boron for protons was determined by scattering monoenergetic protons from a tungsten target on which a thin layer of B[10] had been deposited. For a fixed incident energy, the energy of the protons which emerged from the boron layer after scattering from the tungsten backing was determined to $\pm 0.3\%$ from the midpoint of the step due to tungsten in a profile of the target (Fig. 6). The energy of the protons scattered from a clean tungsten target was determined in the same way at the same incident energy. The difference in the energies of the protons scattered from the tungsten in the two targets is just the energy lost by the protons in the boron layer, with a small correction for the recoil given the tungsten atoms.

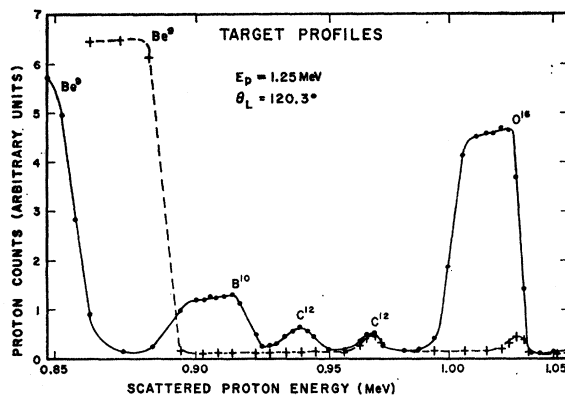The energy loss, ΔE, is related to the stopping cross

FIG. 5. Profiles of a beryllium target and a target of B_2O_3 enriched to 94% B[10], evaporated onto beryllium. The two C[12] peaks on the B_2O_3 target are attributed to pump oil on the front surface of the B_2O_3 and on the beryllium surface behind the B_2O_3.

section by

$$N\Delta x = -\int_{E}^{E-\Delta E} (dE/\epsilon) = \Delta E/\epsilon(E_m),$$

where N is the number of stopping atoms per unit volume of stopping material, Δx the path length of the protons in the boron layer, and $\epsilon(E_m)$ the stopping cross section at some effective energy E_m between the incident energy E and $E - \Delta E$. The energy E_m was calculated by assuming that the stopping cross section is a linear function of energy over the energy thickness of the layer, an approximation valid to within 1% for the small ΔE (less than 10% of the incident proton energy) used in this experiment. The variation of ΔE with E_m for a given target determines the energy dependence of the stopping cross section.

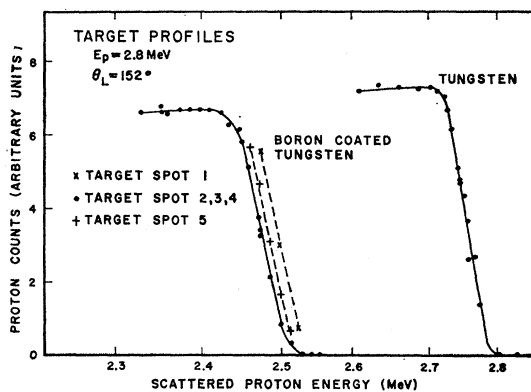To determine the absolute value of the stopping cross section, the number of stopping atoms per unit

FIG. 6. Target profiles showing the tungsten step for a clean tungsten target and for a boron-coated tungsten blank. Uniformity in the thickness of the boron deposit is demonstrated by the position of the tungsten step as a function of the bombarded position on the target. Target spots No. 1 and No. 5 are near the edge of the boron deposit.

TABLE I. The atomic stopping cross section of boron for protons.

Proton energy (MeV)	$(10^{-15}$ eV-cm$^2)$	Proton energy (MeV)	$(10^{-15}$ eV-cm$^2)$
0.099	13.82	0.925	4.28
0.145	12.50	1.133	3.79
0.190	11.13	1.341	3.42
0.235	10.06	1.544	3.09
0.282	9.02	1.746	2.78
0.336	8.22	1.805	2.72
0.379	7.61	1.949	2.54
0.426	7.15	2.152	2.45
0.471	6.82	2.354	2.26
0.523	6.27	2.558	2.14
0.573	5.78	2.642	2.10
0.623	5.66	2.760	2.02
0.717	5.07	2.963	1.99
0.821	4.65		

area of target, $N\Delta x$, must be determined, which, in turn, requires knowledge of both the area and weight of the stopping layer. The area was determined by limiting the boron layer during the deposition process with a circular mask of known area. The diameter of the deposit, which was clearly visible on the backing, was also measured with a traveling microscope. The areas determined by these two methods agreed within 1%.

To determine the weight of the deposit, the sequence of weighing the tungsten blank, heating it in vacuum, and reweighing it, was repeated until the blank reached constant weight. Boron was then deposited and the target reweighed. With an optical lever microbalance, the weight of the boron deposit could be determined with an accuracy of 1%. Diffusion of boron into the tungsten during the deposition process can increase the weight of the target without increasing the thickness of the surface layer. Diffused boron will increase the stopping cross section per tungsten atom and reduce the yield of protons scattered from tungsten atoms at the target surface. Measurements of the scattering yield as a function of depth indicate that the amount of boron diffused in the tungsten was less than 1% of the total amount deposited. The atomic weight of the enriched boron, which enters into the determination of the number of atoms per unit area of target, was calculated from the composition given by the supplier of the B^{10} enriched complex.

The uniformity of the thickness of the deposit was investigated by measuring the position of the tungsten step in the target profile at different positions on the target, as shown in Fig. 6. The thickness was found to be constant within 1% except at the extreme edges of the deposit. The nonuniformity at the edge introduces an uncertainty in the thickness of the target of less than 2%.

The amount of surface contamination on the surface of the boron target was investigated directly by lowering the incident beam energy to such a point that the protons scattered from the contaminants were visible in front of the tungsten step. From this measurement,

the energy loss of protons in the contamination layer was found to be less than 1% of that in the boron layer.

The stopping cross section as a function of proton energy is given in Table I. The compounded probable error due to the sources listed above is estimated at ±4%. The values reported here are in good agreement with unpublished values recently obtained for the stopping cross section for alpha particles in boron.[12] When these measurements with alpha particles are converted into atomic stopping cross sections for protons, with proton energies between 0.125 and 1.0 MeV, they agree within 2% with the values given in Table I.

V. $B^{10}(p,\alpha)Be^7$

An excitation function for the alpha decay to the ground state of Be^7 was measured at a laboratory angle of 90° for proton energies from $E_p=1.5$ to 2.6 MeV. The procedure followed was the same as that used to determine the scattering cross section. Doubly-charged alpha particles were counted at the top of the step in the momentum spectrum of alpha particles from a thick target, and background due to alpha particles from the $B^{11}(p,\alpha)Be^8$ reaction, occurring deep within the target, was determined at the base of the step. The yield was corrected for the number of undetected singly charged alpha particles with the He^+/He^{++} ratios given by Allison,[13] then converted to a cross section with Eq. (1). For this measurement the spectrometer resolution was decreased to approximately 0.8% in energy, and the quantity K of Eq. (1) was determined from the yield of protons elastically scattered by B^{10}.

Values of the $B^{10}(p,\alpha_0)Be^7$ differential cross section at 90° in the laboratory are shown in Fig. 7. The uncertainty in the cross section is estimated to be ±10%. This uncertainty arises largely from the quantity K and is systematic. The energy dependence depicted in Fig. 7 is much more accurate; our estimate of the nonsystematic uncertainty is ±2%.

VI. ANALYSIS METHODS

The R-matrix formalism of Lane and Thomas[14] leads to the following expression for the differential scattering cross section, $d\sigma/d\Omega$, expressed in terms of the classical Coulomb scattering cross section R:

$$\frac{d\sigma/d\Omega}{R} - 1 = \sum_L B_L \frac{P_L(\cos\theta_c)}{k^2 R}$$

$$+ \sum_l (C_l \cos\xi + D_l \sin\xi)\frac{P_l(\cos\theta_c)}{k\sqrt{R}}, \quad (2)$$

[12] We wish to thank Dr. D. Kamke and Dr. P. Kramer of the Physikalisches Institut, Marburg/Lahn, for making these results available to us.

[13] S. A. Allison, Revs. Modern Phys. 30, 1137 (1959).

[14] A. M. Lane and R. G. Thomas, Revs. Modern Phys. 30, 257 (1958).

where $P_L(\cos\theta_c)$ and $P_l(\cos\theta_c)$ are Legendre polynomials, θ_c is the scattering angle in the center-of-mass system, k is the wave number of relative motion for the colliding particles, L is a summation index limited by the values of the orbital angular momentum, $l\hbar$, and ξ is a phase shift given by $\xi=\eta \ln \csc^2(\theta_c/2)$, where η is the Coulomb field parameter. The coefficients B_L, C_l, and D_l, which are functions of the collision matrix, can be expressed in terms of the $B_L(\alpha's',\alpha s)$ and elements of the T matrix which are defined by Lane and Thomas [Eqs. (VIII, 2.7) and (VIII, 2.3) of reference 14]:

$$B_L=\tfrac{1}{4}(2I_1+1)^{-1}(2I_2+1)^{-1}\sum_{ss'} B_L(\alpha s',\alpha s),$$

$$C_l=(2I_1+1)^{-1}(2I_2+1)^{-1}\sum_{Js}(2J+1)\ \mathrm{Im}[T_{slsl}{}^J],$$

$$D_l=-(2I_1+1)^{-1}(2I_2+1)^{-1}\sum_{Js}(2J+1)\ \mathrm{Re}[T_{slsl}{}^J].$$

The terms of Eq. (2) involving C_l and D_l represent interference between Coulomb and nuclear scattering, and the terms involving B_L represent contributions from pure nuclear scattering.

If the summations in Eq. (2) are cut off at finite values of L and l, the various terms are linearly independent functions of angle, and it is possible, at least in principle, to determine the coefficients B_L, C_l, and D_l from the measured angular distributions. The Caltech Burroughs 220 digital computer was programmed to extract the coefficients from the experimental data by the method of least squares with the following sets of values for the summation indices L and l: (1) $L=0$, $l=0$; (2) $L=0$, 1, and 2, $l=0$ and 1; (3) $L=0$, 2, and 4, $l=0$ and 2; and (4) $L=0$, 1, 2, 3, and 4, $l=0$, 1, and 2. Unfortunately, the experimental accuracy was sufficient only to indicate those regions of energy where the scattering might be explained by predominately s-wave scattering processes (case 1). Evaluation of the s-wave least-squares fit by a χ^2 goodness-of-fit test indicated that there was little likelihood of explaining the scattering in terms of $l=0$ processes alone in the energy range from $E_p=1.8$ to 2.8 MeV. For proton energies both above and below this interval, the likelihood increased; the best agreement between the experimental and theoretical scattering for $l=0$ processes was obtained between $E_p=0.4$ and 1.3 MeV.

We have also attempted to fit the energy variation of the scattering cross section. We assume that interference takes place only between levels of different spin and parity, and that potential scattering is independent of the total angular momentum J although dependent on the value of l. In this approximation, elements of the collision matrix have the form:

$$U_{s'l'sl}=e^{i(\omega_l-\phi_l)}e^{i(\omega_{l'}-\phi_{l'})}$$

$$\times\left[\delta_{s'l'sl}+\frac{i\alpha_{sl}{}^J\alpha_{s'l'}{}^J(\Gamma_{pl}{}^J\Gamma_{pl'}{}^J)^{1/2}}{E_\lambda+\Delta_\lambda-E-i\Gamma_T{}^J/2}\right],$$

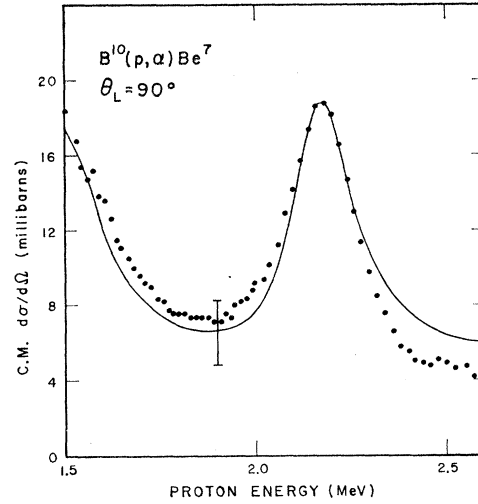
FIG. 7. The differential center-of-mass cross section at a laboratory angle $\theta_L=90°$ for the reaction $B^{10}(p,\alpha_0)Be^7$ is shown as a function of proton energy. The theoretical curve is drawn for level parameters determined from the elastic scattering. The bar at $E_p=1.9$ MeV indicates the possible effect of interference between the levels, when the proton potential scattering phase shifts are determined from hard sphere values.

where ϕ is the potential scattering phase shift; ω_l is the Coulomb phase shift relative to that for $l=0$, given by

$$\omega_l=\sum_{n=1}^{l}\tan^{-1}(\eta/n);$$

$\Gamma_{pl}{}^J$ is the proton partial width of the state with spin J formed by protons with orbital angular momentum $l\hbar$, and $\Gamma_T{}^J$ is the total width of the state. The channel spin mixing parameter $\alpha_{sl}{}^J$ is subject to the condition $\sum_s(\alpha_{sl}{}^J)^2=1$. In evaluating the collision matrix elements, we assume that the Thomas level shift Δ_λ is a linear function of proton energy over the resonance, and absorb this energy dependence in the definitions of the widths and the resonant energy, $E_R=E_\lambda+\Delta_\lambda$. The energy dependence of the penetrability factors in the proton width and total width is considered explicitly.

As a first step in fitting the observed scattering anomalies, the energy dependence of the cross section due to a number of sample levels with a variety of resonance parameters was computed. In those cases where little was known about the properties of the compound state, these examples served as a guide in estimating likely values of the resonance parameters for the observed anomalies. For those states where there was some prior knowledge of the resonance parameters, initial approximations to the parameters for the observed anomalies were chosen to be consistent with at least one of the previous reaction experiments. These parameters were then varied to gain the best fit between experimental and theoretical excitation functions. In these calculations, the potential scattering phase shift was approximated by the hard-sphere value: ϕ_l

$= \tan^{-1}(F_l/G_l)_a$. Following the sign convention of Lane and Thomas, ϕ_l is the negative of the usual hard-sphere phase shift. The nuclear radius, a, was taken to be $a = 1.4(A_1^{1/3} + A_2^{1/3}) \times 10^{-13}$ cm. Values of ϕ_l were also varied from this first approximation value in attempting to obtain the best fit.

VII. RESULTS

A. $E_p < 0.7$ MeV

For proton energies below 700 keV, the scattering angular distributions can be reproduced reasonably well by assuming that only s-wave potential scattering occurs. The best theoretical curves for this assumption are indicated by the curves in Fig. 2, and the phase shift ϕ_0 is shown in Fig. 8. There are several reasons for questioning the interpretation that the scattering can be adequately described by s-wave potential scattering only. Neither the value nor the energy dependence of ϕ_0 agrees with that due to scattering by a hard sphere. This in itself might not be considered a serious objection since the phase shifts are small and quite dependent on inaccuracies in the cross sections. If, however, the excitation curves are plotted with a condensed energy scale, it becomes apparent that the cross section at 90° exhibits behavior expected from a resonant state formed by $l=1$ protons, with a resonant energy and total width of approximately 270 keV and 70 keV, respectively. Unfortunately, the excitation functions at other angles show no anomaly and it was not possible to fit them with level parameters which simultaneously fit the behavior at 90°. Since the anomaly at 90° is only two or three times the statistical error, it would be tempting to ascribe this behavior to some systematic error, except that the previously reported state at $E_x = 8.97$ MeV should appear at approximately this proton energy. Although the best agreement with theory is obtained with $l=0$ potential scattering, the possibility of a state influencing the cross section in this energy region cannot be excluded.
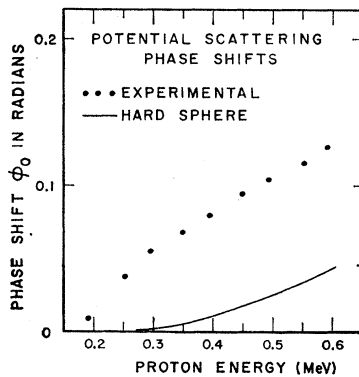

FIG. 8. Values of the experimentally determined s-wave potential scattering phase shift ϕ_0 as a function of proton energy. Also shown are the hard sphere values of ϕ_0 for a radius of 4.4 $\times 10^{-13}$ cm.

There is no evidence in the scattering for the states reported at $E_x = 9.13$ and 9.28 MeV. If these states exist, their total widths must be less than 2 keV, or the ratio of the proton partial width to the total width, Γ_p/Γ_T, less than 0.05.

B. $0.7 < E_p < 1.7$ MeV

For proton energies greater than 0.7 MeV the scattering cannot be explained in terms of potential scattering alone. Resonance parameters were first estimated for the conspicuous anomaly near $E_p = 1.5$ MeV by comparing the energy dependence of the observed cross section with that computed for sample cases. This comparison suggests that the state at $E_x = 10.09$ MeV is formed predominantly by s-wave protons, thereby limiting the spin and parity to $J^\pi = 5/2^+$ or $7/2^+$. Of these two, the $7/2^+$ assignment is consistent with the results of other experiments. Indeed, the magnitude of the step in the cross section can be reproduced at all angles with the following resonance parameters which Cronin[5] deduced from his studies of the alpha decay of this state: $J^\pi = 7/2^+$, $\Gamma_{p0} = 76$ keV, $\Gamma_{p2} = 14$ keV, $\Gamma_{\alpha_0} = 100$ keV, $\Gamma_{\alpha_1} = 60$ keV, and $\Gamma_T = 250$ keV. The scattering indicates a resonant energy of $E_R = 1.50 \pm 0.02$ MeV. The nature of the fit is not strongly dependent on the channel spin mixing parameter for d-wave formation of the state.

The angular distributions of scattered protons cannot be fit by considering the contribution of the $7/2^+$ state alone. Interference with neighboring states must be considered, and it is reasonable to expect the broad state at $E_p = 1.17$ MeV to influence the angular distributions. We have computed angular distributions arising from the interference of three sources of scattering: hard-sphere scattering; resonant scattering through a state at $E_p = 1.5$ MeV ($E_x = 10.09$ MeV) with the properties listed above, and through a state at $E_p = 1.17$ MeV ($E_x = 9.76$ MeV). A variety of possible parameters for the latter state consistent with the resonant α_0-particle cross section ($\sigma = 4\pi \times 6 \times 10^{-27}$ cm^2) measured by Cronin at $E_p = 1.17$ MeV are listed in Table II. Angular distributions were computed for each of these possible assignments of parameters for the 9.76-MeV state.

In the energy range $0.7 \leq E_p \leq 1.3$ MeV, the observed angular distributions can be fit with the $5/2^+$, $\Gamma_{p0} = 0.045$ MeV choice for the 9.76-MeV state. A theoretical curve for this hypothesis is shown in Fig. 9 with an experimental angular distribution. For the other possibilities of Table II, the agreement is less satisfactory; the next best fit is obtained with the parameters $5/2^-$, $\Gamma_{p1} = 0.045$ MeV, also shown in Fig. 9. A $3/2^-$ assignment gives even poorer agreement because of the increased ratio Γ_p/Γ_T.

For $E_p > 1.3$ MeV, the angular distributions could not be fit with any of the possible parameters listed in Table II for the 9.76-MeV state, and we must assume

TABLE II. Possible resonance parameters for the state at $E_p = 1.17$ MeV, with $\Gamma_T = 300$ keV.

J^π	Γ_p (MeV)	Γ_{α_0} (MeV)
$3/2^-$	0.075	0.225
	0.225	0.075
$5/2^-$ or $5/2^+$	0.045	0.255
	0.255	0.045

that other states contribute to the background in this energy region. (The results of our χ^2 test also indicate that protons with $l > 0$ take part in the scattering for $E_p > 1.3$ MeV.) We believe, however, that failure to reproduce the angular distributions in the neighborhood of $E_p = 1.5$ MeV does not cast doubt on our assignment for the state at this energy, which is based on the magnitude of step in the excitation function. The theoretical fit to this step is shown in Fig. 3; the curve is drawn for the $5/2^+$ assignment for the state at $E_p = 1.17$ MeV, but the shape is relatively independent of the properties of the state at lower energy.

C. $E_p > 1.70$ MeV

Comparison of the observed cross section near $E_p = 2.2$ MeV with the patterns produced by sample levels suggests that this anomaly is due predominantly to protons with $l = 2$. Of the spin values which can be formed by combining the spin of $B^{10}(3^+)$ with d-wave protons, the $9/2^+$ and $11/2^+$ assignments are the only ones which can be made exclusively with $l = 2$ protons, and which also provide an obvious reason for the nonresonant behavior of the low-energy α_1 group, since either of these assignments require angular momentum $l_\alpha = 5$ for the decay to the first excited state of Be^7. If the assignment were $J^\pi = 11/2^+$, a large width for the α_0 transition to the ground state of Be^7 would be necessary, inconsistent with an orbital angular momentum of $l = 5$ required for this decay. Theoretical excitation curves for the $9/2^+$ assignment are shown in Fig. 3, with $E_R = 2.180$ MeV, $\Gamma_{p2} = 100$ keV, and $\Gamma_T = 200$ keV. The $J^\pi = 9/2^+$ assignment requires that the α_0 decay be resonant, with a partial width of 100 keV for α_0 particles with orbital angular momentum $l = 3$. This reaction is indeed resonant near $E_p = 2.180$ MeV, as shown by the $B^{10}(p,\alpha_0)$Be^7 excitation function of Fig. 7. The theoretical curve shown in Fig. 7 was obtained by using for the 10.09- and 10.68-MeV states the parameters obtained from the scattering analysis, except that we assumed (1) a constant background of 3.7 mb over this entire energy range; (2) that the 10.09-MeV state is formed by s-wave protons only, with a proton width $\Gamma_{p0} = 90$ keV; and (3) that the 10.68-MeV state is formed exclusively by channel spin 5/2 protons. Without altering the fit of the theoretical curve at resonance, the agreement can be improved between the resonances by assuming some channel spin 7/2 formation of the 10.68-MeV state, thus introducing
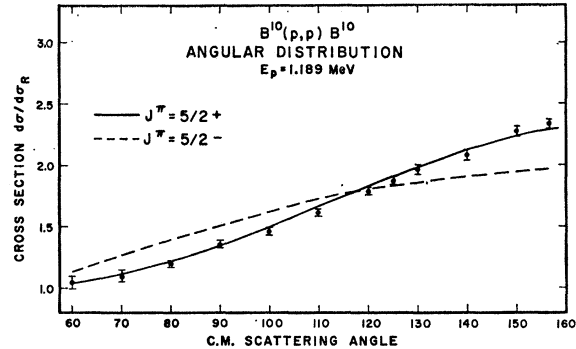

FIG. 9. The scattering angular distribution at $E_p = 1.189$ MeV. The theoretical curves are for states assumed resonant at $E_p = 1.17$ MeV with $J^\pi = 5/2^+$ and $J^\pi = 5/2^-$, superimposed on a background of potential scattering and contributions from the $J^\pi = 7/2^+$ state at $E_p = 1.50$ MeV.

interference between the α_0 decays of the two states. The possible effects of interference, assuming a proton potential scattering phase shift given by the hard-sphere value, are also shown in Fig. 7. A detailed calculation of the interference was not performed because of the possibility of interference with the unknown background. The height of the peak at $E_p = 2.180$ MeV limits the spin of the state to values larger than 5/2.

In order to obtain the theoretical curve shown in Fig. 3 above $E_p = 1.9$ MeV, it was necessary to assume the presence of a still higher state, formed predominantly by s-wave protons. We assumed a state at $E_R = 2.82$ MeV, to agree with the previously reported state at $E_x = 11.26$ MeV. The parameters used for this state were: $J^\pi = 7/2^+$, $\Gamma_{p0} = 192$ keV, $\Gamma_{p2} = 48$ keV, and $\Gamma_T = 600$ keV. At these energies there are many sources of background which can contribute to the scattering (for example, the state previously reported at $E_p = 2.40$ MeV, $E_x = 10.89$ MeV, but not observed here) and we do not claim that the parameters assumed for the 11.26-MeV state are the only ones consistent with the scattering measurements. The assumption of an s-wave state at this energy is consistent with the results of the least-squares analysis, since the likelihood of a good s-wave fit increases above $E_p = 2.60$ MeV.

VIII. CONCLUSIONS

For proton energies below $E_p = 0.7$ MeV, the scattering can be explained in terms of pure s-wave potential scattering, but the possibility of a state near $E_p = 0.270$ MeV, corresponding to an excitation energy $E_x = 8.95$ MeV in C^{11}, cannot be excluded. At higher proton energies, all experimental results permit consistent assignments for states near $E_p = 1.50$ MeV $(E_x = 10.06$ MeV$)$ and $E_p = 2.180$ MeV $(E_x = 10.68$ MeV$)$. The properties of these states are summarized in Table III. The dimensionless reduced widths $\theta^2 = \gamma^2 [2Ma^2/(3\hbar^2)]$ for these states do not violate the

TABLE III. Level parameters for the states of C^{11}.

E_x (MeV)	J^π	E_R (MeV)	Γ_p (MeV)	Γ_{α_0} (MeV)	Γ_{α_1} (MeV)	θ_p^2	$\theta_{\alpha_0}^2$	$\theta_{\alpha_1}^2$
10.06	7/2+	1.50	0.090	0.100	0.060	0.02	0.26	0.35
10.68	9/2+	2.18	0.100	0.100	⋯	0.17	0.11	⋯

Wigner sum rule limits.[15] The previously reported states in C^{11} at excitation energies $E_x = 9.13$, 9.28, and 10.89 MeV are not observed, but there is evidence for a state formed by s-wave protons near $E_p = 2.8$ MeV ($E_x = 11.24$ MeV).

The confusion regarding the state at $E_x = 9.76$ MeV is not clarified by our scattering measurements which require even parity for this state, while the (p,α) and (p,γ) experiments have been interpreted to indicate a state of odd parity. In spite of this contradiction, we contend that all three reactions demonstrate some consistency with the interpretation that for $E_p \leq 1.2$ MeV the reactions are fed with s-wave protons. Furthermore, all three reactions indicate that protons of higher orbital momenta take part for $E_p > 1.3$ MeV. The evidence is clear in the $B^{10}(p,p)B^{10}$ results: A good fit to the scattering angular distributions with s-wave protons is obtained below 1.3 MeV; above this energy the fit becomes progressively worse. In the $B^{10}(p,\alpha_0)Be^7$ reaction, the α-particle isotropy for $E_p \leq 1.2$ MeV, and the peaking of $P_1(\cos\theta)$ and $P_3(\cos\theta)$ interference terms at $E_p = 1.36$ MeV, are in agreement with this interpretation. In the $B^{10}(p,\gamma)C^{11}$ reaction, the energy dependence of the excitation function for the ground-state transition fits the energy dependence of an s-wave barrier penetration factor for $E_p \leq 1.0$ MeV. If the s-wave barrier factor is extracted, the resulting cross

---

[15] T. Teichman and E. P. Wigner, Phys. Rev. **87**, 123 (1952).

---

section exhibits interference phenomena for $E_p > 1.2$ MeV.

Some time ago, Brown et al.[6] suggested a possible explanation for this behavior when they proposed that the α_0-particle excitation curve might be explained by a resonant $J^\pi = 3/2^-$ state superimposed on a broad $J^\pi = 5/2^+$ state in C^{11}. If the $J^\pi = 5/2^+$ state were resonant near $E_p = 1.17$ MeV and an odd-parity state were resonant near $E_p = 1.35$ MeV, all of the behavior described above could be qualitatively understood, as could the present disparity in the total width and the slight (though hardly significant) difference in resonant energy of the $E_x = 9.76$ MeV state obtained from the $B^{10}(p,\alpha)Be^7$ and $B^{10}(p,\gamma)C^{11}$ experiments.

Since the primary objection to such an interpretation arises from the anisotropy in the γ-ray angular distributions, the best way of testing this hypothesis is through further study of the gamma transition to the ground state of C^{11} for proton energies from $E_p = 1.0$ MeV to $E_p = 1.5$ MeV. The odd-parity state should be observed as a small anomaly superimposed on the broad resonance already known to exist, or as a small $\cos\theta$ anisotropy in the angular distributions. If such effects are observed, they should be more amenable to analysis than the results of the other proton-induced reactions for threre should be no confusion resulting from the $J^\pi = 7/2^+$ state at $E_p = 1.5$ MeV.